THE ASTROPHYSICAL JOURNAL, 236:1035–1042, 1980 March 15

A STUDY OF THE JOVIAN [S II] NEBULA AT HIGH SPECTRAL RESOLUTION[1]

J. T. TRAUGER
Division of Geological and Planetary Sciences, and Jet Propulsion Laboratory, California Institute of Technology
G. MÜNCH
Max-Planck-Institut für Astronomie, Heidelberg
AND
F. L. ROESLER
Department of Physics, University of Wisconsin, Madison
Received 1979 August 6; accepted 1979 September 20

ABSTRACT

Observations of [S II] λλ6716–6731 emissions from the Jovian magnetosphere have been carried out with a PEPSIOS spectrometer at the Hale 5 m telescope. Spectral resolving power was sufficient to resolve the [S II] line widths. From measured λλ6716–6731 doublet ratios and spectral line widths we found a thermal plasma characterized by temperatures $\sim 2 \times 10^4$ K and electron densities $\sim 2 \times 10^3$ cm^{-3}. The source of [S II] emissions was centered within a toroidal region of radius 5 R_J (inside the orbit of Io), with tight latitudinal confinement near the equilibrium equator for ions in the tilted corotating Jovian magnetic field, and significant long-lived longitudinal structure.

Subject headings: planets: Jupiter

I. INTRODUCTION

The presence of S^+ ions in the magnetosphere of Jupiter, discovered by Kupo, Mickler, and Eviatar (1976) offers the opportunity to make ground-based optical measurements of the physical state of the Jovian magnetospheric plasma (Brown 1976). The extended nature and low surface brightness of the [S II] emitting regions suggest that Fabry-Perot instrumentation would be ideal for its spectrophotometric study at high spectral resolution. This paper reports measurements of the [S II] λλ6716–6731 doublet obtained during 1976 October 7–11 with a triple Fabry-Perot PEPSIOS spectrometer at the Mount Palomar 5 m telescope, and follows the preliminary report of Münch, Trauger, and Roesler (1977).

In §§ II and III of this paper we describe our program of observations and direct quantitative results, including spatial characteristics in the observed emission strengths, line widths place direct constraints upon the ion temperatures, and wavelengths and velocity shifts in the observed emissions. In § IV we interpret these data in terms of thermal plasma characteristics, to obtain electron and ion temperatures and densities and implications for the confinement geometry. In § V we discuss these results and their meaning for the overall Jovian magnetospheric properties.

II. INSTRUMENTATION AND PROGRAM

The spectrometer was configured for a spectral resolving power of 110,000 and a 34″ diameter field of view (FOV) in the sky, equivalent to a diameter of 1.5 Jovian radii (R_J). The FOV was positioned relative to the coudé image of Jupiter on a polar coordinate grid concentric with the FOV, and the accuracy of this procedure for centering and guiding is estimated to have been within 5″, sufficient in relation to the large FOV diameter. We followed a flexible observing program using an analog readout of the observed spectra to modify our program according to indications or trends as they appeared. More complete information was extracted afterward by computer processing of the digital records.

The line profiles were sampled in consecutive wavelength channels of 0.0088 Å width, measured by fringes of a reference Michelson Interferometer. The corresponding integration time per channel was about 20 s. Wavelengths were calibrated against the Ne I λ6716.042 line. The first observations, carried out 1976 October 7, unmistakably revealed the presence of the λ6717 line on each of six scans obtained with the field centered on the rotational equator, and at a distance from Jupiter $\delta = 0.75$ in units of the apparent radius of the Io orbit (i.e., $\delta = 1.0$ corresponds to 5.9 R_J). Peak emission was observed near the wavelength expected for material corotating with the Jovian magnetic field. No significant signal could be detected at $\delta = 1.0$ (four scans) or at $\delta = 0.5$ (one scan). The detection of [S II] near the corotation velocity suggested that a Doppler compensating, off-axis Fabry-Perot adjustment would be appropriate (Trauger and Roesler 1972), because spectra obtained with such an alignment reveal velocity structure within the corotating frame, unobscured by systematic Doppler shifts amounting to 17.5 km s^{-1} across our FOV due

[1] Contribution No. 3305 of the Division of Geological and Planetary Sciences, California Institute of Technology.

to rigid corotation with Jupiter. A total of 67 scans including both [S II] lines were obtained during October 7–11 at various radial distances δ from Jupiter and a sampling of various zenocentric latitudes and longitudes. The quality of the profiles obtained is shown in Figure 1, which displays five representative pairs of line profiles, each consisting of two consecutive scans obtained within 20 minutes, and a sequence of five consecutive scans. The continuous curves shown superposed on the histogram presentation of the raw data are least-squares fitted Gaussian profiles. The parameters free to vary in the fitting process were the level of background continuum (primarily due to scattered light from Jupiter, but also including the detector dark count), the wavelength at which peak emission occurs, h = height above the continuum of maximum emission, and w = full width at half-maximum (FWHM) emission. The emission rate E in Rayleighs (1 Rayleigh = 10^6 photons cm^{-2} s^{-1}) corresponding to a Gaussian line with parameters h and w, from a source uniformly filling the solid angle of acceptance Ω, observed with a telescope of collecting area A and an optical system of net absolute efficiency ϵ (counts per photon) is obtained from

$$E = \frac{2\pi S}{\epsilon A \Omega}\left(\frac{\pi}{\ln 2}\right)^{1/2} hw\,.$$

The values of ϵ for both [S II] lines were obtained by measuring the power of spectrophotometric standard stars. The values of E in Rayleighs and deconvolved [S II] line widths in km s^{-1} for all the scans obtained are given in Table 1, where they are identified by their decimal date. Emission rates have been corrected for atmospheric extinction. An instrumental width of 2.9 km s^{-1}, determined with reference to a Thorium calibration line from a hollow cathode lamp, is deconvolved from the listed line widths under the assumption that both the instrument and the thermally broadened [S II] lines are Gaussian in form.

Error limits in the determination of emission rates from individual scans have been estimated in the usual way in terms of the statistical noise level and fitted line parameters, and are similar for all scans because of similar noise levels throughout the data set. Upper limits in several scans with undetected lines were derived by the same statistical procedure with model line widths fixed at a representative FWHM. In all cases a standard deviation of about 5 Rayleighs is found, and in the following sections confidence limits of ± 10 Rayleighs and upper limits of 10 Rayleighs are quoted for individual determinations of the FOV–averaged emission rates.

III. RESULTS

a) *Emission Rates*

The [S II] emission rates listed in Table 1 may be inspected for their dependence on the distance δ of the FOV from Jupiter, on the latitudes φ_c and System III (1965) longitudes l_{III} of the FOV, and for time variabilities. Here the latitude φ_c is the angular devia-

TABLE 1

SELECTED RESULTS AND PARAMETERS FOR INDIVIDUAL [S II] SPECTRA

Date (UT)	E (Rayleigh)	w (km s^{-1})	δ	l_{III} (1965)	φ_c
7.292...	< 10*	...	1.00W	302°	−1°.6
7.319...	< 10*	...	0.50W	327	−4.3
7.340...	84*	9.8	0.75W	345	−5.8
7.358...	54*	7.7	0.75W	360	−6.7
7.375...	93*	12.7	0.75W	15	−7.1
7.396...	55*	12.7	0.75W	33	−6.7
7.434...	< 10*	...	1.00E	66	−4.8
7.451...	< 10*	...	1.00E	81	−3.3
7.472...	65*	6.5	0.75W	100	−1.2
7.493...	64*	7.3	0.75W	118	+1.0
7.517...	< 10*	...	1.00W	139	+3.5
9.289...	35*	7.3	0.75W	241	+5.3
9.303...	19*	2.6	0.75W	253	+4.2
9.319...	38	5.1	0.75W	267	+2.6
9.333...	32	6.0	0.75W	280	+1.2
9.358...	34*	7.3	0.75W	301	−1.4
9.375...	35*	7.3	0.75W	316	−3.2
9.389...	61	7.3	0.75W	328	−4.4
9.403...	55	8.6	0.75W	340	−5.5
9.424...	< 10	...	0.50W	358	−6.6
9.438...	35	10.6	0.50W	10	−7.0
9.448...	37	9.8	0.50W	19	−7.1
9.469...	< 10	...	1.00W	37	−6.7
9.483...	< 10	...	0.88W	49	−6.1
9.496...	41	10.6	0.88W	61	−5.3
9.514...	56	9.8	0.75W	77	−3.8
9.524...	38	6.9	0.75W	86	−2.8
9.538...	6	...	0.63W	98	−1.4
10.234...	42	9.0	0.75E	164	+5.7
10.250...	17	9.0	0.75E	177	+6.6
10.265...	63	5.6	0.75E	191	−3.0
10.278...	< 10	5.1	0.75E	202	−12.9
10.290...	49	6.5	0.75E	212	−3.1
10.303...	45	6.5	0.75E	224	−3.6
10.319...	23	6.5	0.75E	237	+0.6
10.340...	24	6.9	0.75E	255	−8.1
10.357...	28	4.7	0.75E	270	−4.7
10.376...	18	4.7	0.75E	287	−4.7
10.388...	19	4.7	0.75E	298	−2.0
10.418...	21	4.2	0.63W	144	+4.0
10.430...	27	4.7	0.63W	154	+5.0
10.444...	40	8.2	0.75E	346	−0.9
10.469...	29	5.6	0.75E	8	−0.9
10.482...	34	4.2	0.75E	19	+0.9
10.510...	46	6.5	0.75E	43	+3.6
10.517...	49	9.4	0.75E	50	+3.9
10.528...	39	8.6	0.75E	60	+4.6
11.226...	43	6.5	0.75W	127	+0.2
11.243...	40	3.7	0.75W	142	+0.8
11.263...	54*	6.5	0.75W	159	+1.4
11.276...	62	3.7	0.75W	171	+0.2
11.288...	61*	6.5	0.75W	181	−0.3
11.297...	67	6.5	0.75W	189	−1.1
11.310...	46*	4.2	0.75W	200	−1.9
11.320...	45	4.7	0.75W	209	−3.0
11.333...	34	3.2	0.75W	220	+4.6
11.344...	8	4.7	0.75W	229	−11.9
11.357...	27	3.7	0.75W	241	−5.7
11.367...	17	2.6	0.75E	250	+4.5
11.377...	33	4.2	0.75W	258	−7.4
11.391...	21	3.2	0.75W	270	−8.7
11.401...	< 10	...	0.63W	279	+1.2
11.478...	9	4.7	0.63W	345	−5.9
11.489...	71	6.0	0.75E	176	+6.5
11.499...	< 10	...	1.00E	184	+6.8
11.510...	52	6.5	0.75E	194	+7.0
11.520...	41	6.0	0.75E	203	+7.0

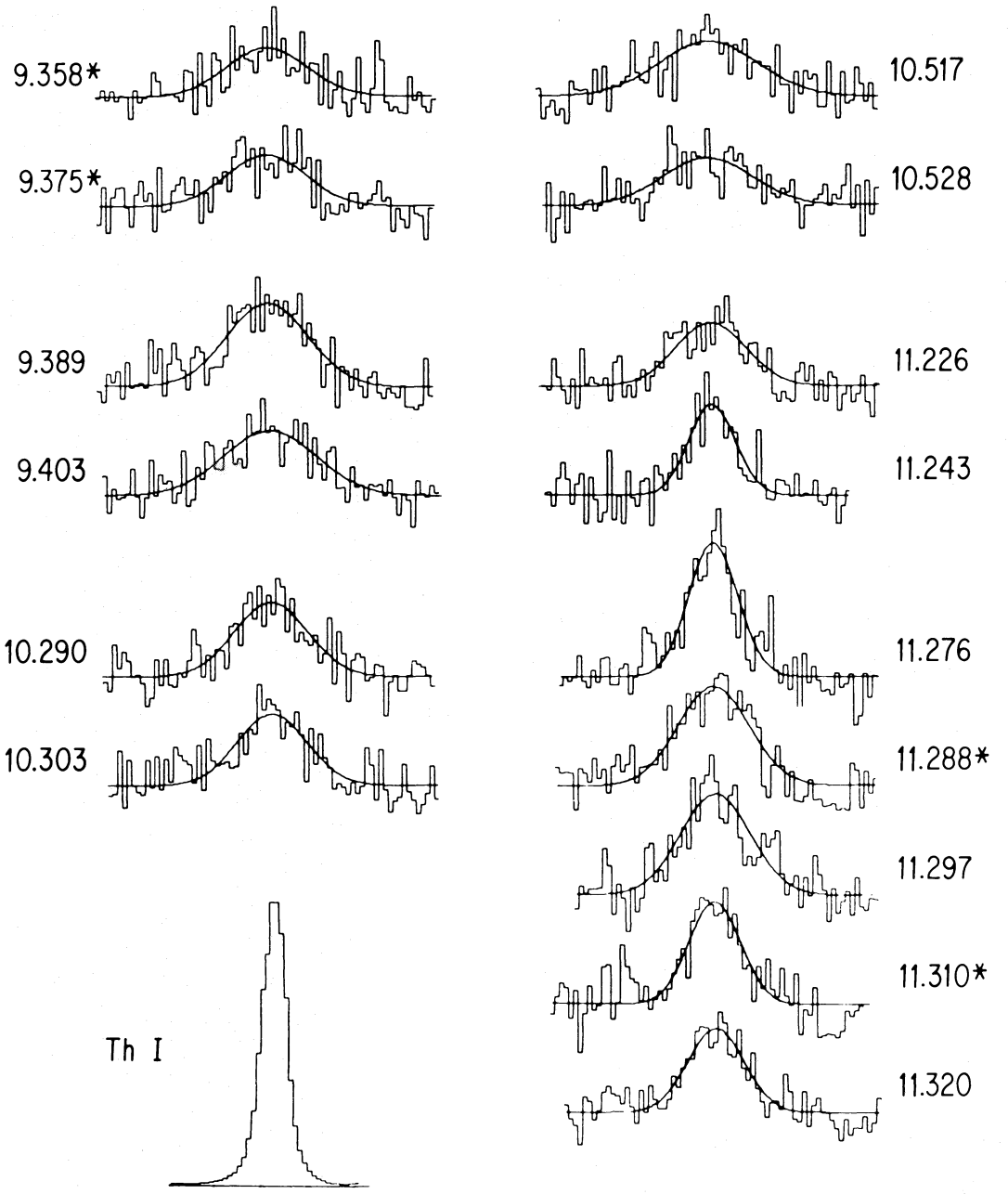

FIG. 1.—Representative [S II] spectra obtained at a radial distance $\delta = 0.75$ from Jupiter. Scans are identified by their decimal date (cf. Table 1), with an asterisk indicating scans of the λ6716.47 line; all others are scans at λ6730.85. Each [S II] spectrum shows a fitted Gaussian profile superposed upon raw photon counting data sampled at 0.0088 Å intervals across the scan. The [S II] line centers occur with Doppler shifts in precise agreement with expectations for rigid corotation with Jupiter. The spectral resolution of our instrument is indicated by a single scan of the Thorium λ6727.46 line from a laboratory lamp. The illustrated scans are a representative random sample of the spectra listed in Table 1, with pairs of scans obtained within 20 minutes or less at similar observing FOV geometry grouped together. The series of five scans (11.276–11.320) taken alternatively at λ6730.85 and λ6716.47 facilitates an estimate of the electron temperatures and densities based on the [S II] doublet ratio (DR), as discussed in the text.

tion of the FOV center from the equilibrium equatorial plane for trapped ions under the combined influence of the tilted Jovian magnetic dipole field and the centrifugal effects of Jovian rotation, as discussed further in § IV*b*. We inspect our data in an attempt to discern general systematics in the observed [S II] emission rates.

On the basis of the announcement of Kupo, Meckler, and Eviatar (1976), we expected to find maximum line intensities at $\delta = 1$. This expectation was not verified by the six scans obtained at $\delta = 1$, which show no evidence for emissions with an upper limit set by statistical uncertainties at $E \lesssim 10$ Rayleighs. Our sampling of the line intensities with a field stop diameter equal to 1.5 R_J at $\delta < 1$ indicates that maximum intensities are found with the FOV centered at $\delta = 0.75$. Only one of the 50 tracings obtained with this δ failed to show a significant emission rate. The mean emission rates at $\delta = 0.75$ and $\varphi_c < 8°$ taken from Table 1, together with their standard deviations, are

$$E(\lambda 6716) = 54 \pm 21 \text{ Rayleighs} \quad (13 \text{ scans}),$$

$$E(\lambda 6731) = 41 \pm 15 \text{ Rayleighs} \quad (33 \text{ scans}).$$

It may be noted that individual scans show variations from these mean intensities larger than the formal errors for individual determination, and that emission rates obtained from consecutive scans with nearly the same observing geometry often agree within 10%, as the data in Table 1 and representative tracings in Figure 1 show.

Significant emission rates for λ6731 were obtained also at other $\delta < 1$, but too few samples were taken for a meaningful statistical average. We list the observed range of values, and note once again that the individual scans show variations among themselves which exceed the formal error limits for single determinations.

$\delta = 0.50$, $E(\lambda 6731) = 0$–37 Rayleighs (3 scans)

$\delta = 0.63$, $E(\lambda 6731) = 0$–27 Rayleighs (5 scans)

$\delta = 0.88$, $E(\lambda 6731) = 0$–41 Rayleighs (2 scans)

Assuming for the moment that the distribution for the source of [S II] emissions is toroidal and axially symmetric about Jupiter, we may infer the radial dependence of the source distribution from the observed δ dependence in our line-of-sight emission rates. The assumption of axial symmetry neglects significant longitudinal and temporal variations clearly evident in the data, but is useful for the characterization of the [S II] source region. The appearance of a representative uniform toroidal source distribution is illustrated in Figure 2, with due consideration for the large FOV in this experiment. The curve in Figure 2 represents a torus centered at 5.0 R_J from Jupiter, which for our observing geometry results in a peak emission rate when the FOV is centered at $\delta = 0.75$ (4.5 R_J). Here the radial thickness of the torus cross section is assumed to be 0.75 R_J, but the peak position

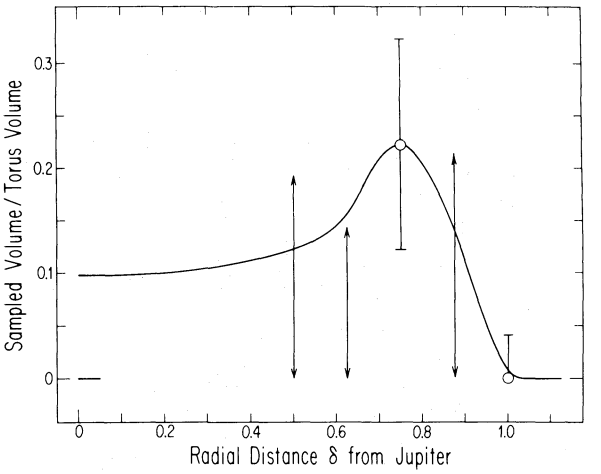

FIG. 2.—Computed volume of a representative equatorial torus sampled by our FOV as a function of radial distance of the FOV center from Jupiter. The assumed toroidal volume is centered at $\delta = 0.84$ from Jupiter (i.e., 5.0 *RJ*), with a radial thickness of 0.75 R_J and a thickness perpendicular to the equatorial plane of 1 R_J. The assumed FOV is a realistic 1.5 R_J in diameter centered on the equator. This curve peaks with the FOV center near $\delta = 0.75$ as suggested by our observations, a result which is not strongly dependent on the assumed thickness of the torus. Shown superposed upon the curve are averaged values of emission rate at $\delta = 0.75$ and 1.00 together with the standard deviations in observed variabilities from these averages. Arrows at $\delta = 0.50$, 0.63, and 0.88 indicate the observed range of emission rates at those distances from Jupiter, for which our data contain an insufficient number of scans for statistical estimates. All data are normalized to give a match to the curve at $\delta = 0.75$.

is not sensitive to this dimension. Relying primarily on the emission rate data at $\delta = 0.75$ and 1.0, we see that a S^+ torus at 5.0 R_J from Jupiter gives the best match to our observations.

The data may be further inspected for dependences upon φ_c. A representative sample of 50 emission rates in both the λ6716 and λ6731 lines at $\delta = 0.75$ are plotted against φ_c in Figure 3. The FOV centers in the October 10–11 data are distributed over all zenocentric latitudes within ±11° of the rotational equator, while the October 7–9 scans are all centered at the rotational equator. Although the information from individual scans is limited by apparent time variabilities, we see little variation in the average emission rates for φ_c within 8° of the centrifugal confinement equator, as would be expected for a thermal plasma tightly confined (within a few degrees in latitude) near the centrifugal equilibrium equator when observed with our large FOV (extending over 19° in latitude at $\delta = 0.75$). The small statistical sample at greater magnitudes of φ_c showing low emission rates also suggests that the emitting region is confined within only a few degrees in latitude. The distribution in [S II] emission rates against either Jovian rotational or magnetic latitudes fails to show such tight confinement.

Finally, we consider the correlation of emission rates with longitudinal position of the line-of-sight volume sampled by our FOV, as illustrated in Figure

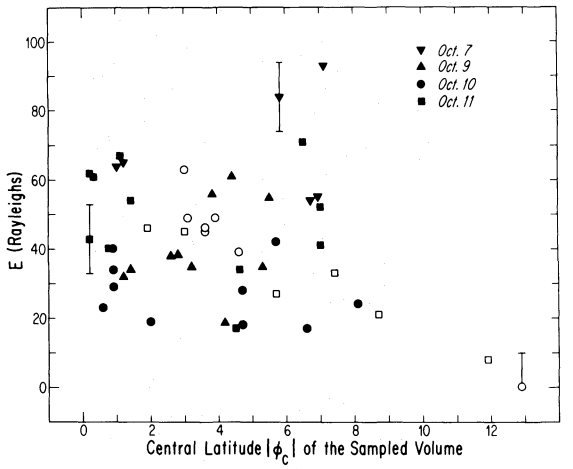

FIG. 3.—Plot of all 50 [S II] emission rates at $\delta = 0.75$ against the angular displacement φ_c of the FOV center from the centrifugal confinement equator. Data from different nights of observing are distinguished by symbol shapes as indicated. Open symbols indicate those scans taken with the FOV center more than 8° from the rotational equator.

4. As in the previous figure, 50 scans taken in both the λ6716 and λ6731 lines at $\delta = 0.75$ are included. It may be noted that our FOV sampled over 20% of the total toroidal volume bounding the [S II] emitting regions (cf. Fig. 2). Thus each data point in the figure represents an integration over a significant fraction of the source region, and small-scale variations in emission rates with longitude would tend to be averaged out. Despite scatter in the data, there is evidence for a pattern in the emission rates which persisted over our entire observing period or about 10 Jovian rotations. A tendency for low emission rates at $l_{III} \sim 280°$ suggests a low brightness segment of the torus extending nearly 90° in longitude and centered at 280°. For reference, the Jovian north magnetic pole is tilted into the 200° meridian in System III (1965) coordinates.

b) *Radial Velocities*

The [S II] lines are found at wavelengths close to those expected for material corotating with the Jovian magnetic field. If the field is assumed to be a centered spin-aligned dipole, the corotation velocity at Io's orbital radius is 74.17 km s^{-1} relative to the center of mass of Jupiter. The departures of the actual Jovian magnetic field (Smith, Davis, and Jones 1976; Acũna and Ness 1976) from the centered spin-aligned geometry are of some relevance (±1.5 km s^{-1}) only with on-axis etalons. In the Doppler-compensated mode, displacements within the FOV of corotating sources produce no wavelength shifts. For the purpose of wavelength determinations, we consider only the Doppler-compensated scans. After allowing for the orbital motions of Earth and Jupiter, we find that the observed position of the λ6731 line in 31 scans with the best-determined line positions is best fitted by adopting a rest wavelength 6730.85 ± 0.02 Å. Similarly, from the mean of five scans for the λ6716 line we find a rest wavelength 6716.47 ± 0.02 Å. The values derived by Bowen (1955) from observations of emission nebulae are 6730.78 ± 0.05 and 6716.42 ± 0.08 Å, respectively. We suggest that the small discrepancy existing between the two determinations arises from uncertainties in the nebular measurements and that the true rest wavelengths for the [S II] red doublet lines are 0.05 Å (+2.2 km s^{-1}) longer than the values given by Bowen (1955).

c) *Line Widths*

The line widths w listed in Table 1, similar to the emission rates, appear not to be constant, but to vary over a range larger than the mean errors of their determination. The values of w obtained with the PEPSIOS in the Doppler-compensated mode have been corrected only for the instrumental profile to derive the true distribution of the velocity components along the line of sight of the emitting ions. From scans of the Th I λ6727.46 line (cf. Fig. 1) it has been

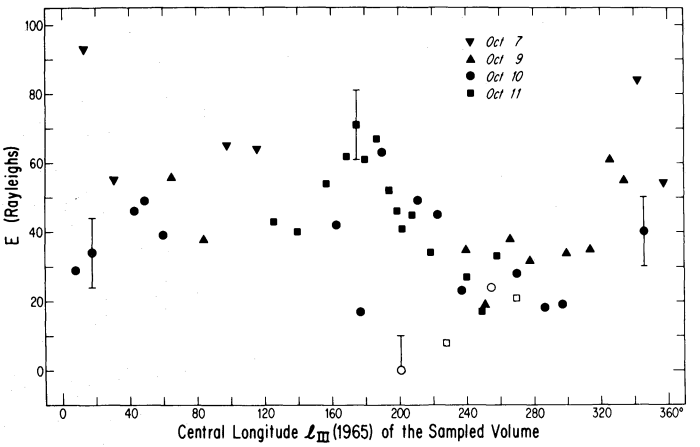

FIG. 4.—Plot of all [S II] emission rates at $\delta = 0.75$ against the System III (1965) longitude of the meridian at the center of the torus volume sampled by our FOV. Symbol shapes are the same as in Fig. 3, with open symbols representing scans for which $|\varphi_c|$ was greater than 8°.

determined that the instrumental profile has a nearly Gaussian form with FWHM = 2.9 km s^{-1}. The mean value and standard deviation of the sample of 39 line profiles with best-determined line widths obtained in the Doppler-compensated mode, after correction for the instrumental profile, is

$$\bar{w}_c = 6.2 \pm 1.5 \text{ km s}^{-1} .$$

These widths provide an upper limit to the S^+ temperature averaged within our FOV, as discussed further in the following section. In comparison, the mean line width for five line profiles obtained with on-axis etalons is

$$\bar{w}_u = 8.8 \pm 2.3 \text{ km s}^{-1} ,$$

a value which is not significantly different from $\bar{w}_c$. The question arises as to how different the line widths of a source in rigid corotation should be when measured in the Doppler-compensated and uncompensated modes. For a uniformly illuminated FOV and a Gaussian distribution of velocities around the corotating mean value, numerical computation predicts a FWHM = 15.3 km s^{-1} with our observational parameters, a value different from $\bar{w}_u$ by almost three standard deviations. This difference provides evidence, in addition to the δ-dependence of E, that our FOV at $\delta = 0.75$ was not filled uniformly by the [S II] emission, but rather concentrated in radial distance from Jupiter.

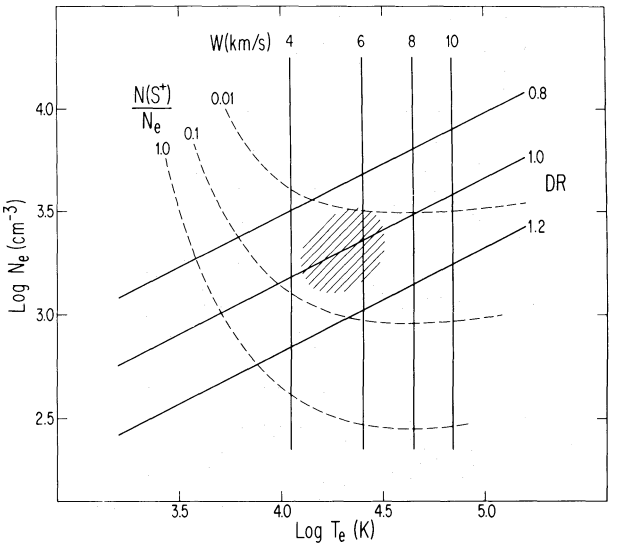

FIG. 5.—Calculated lines of constant doublet ratio DR = $E(\lambda 6716.47)/E(\lambda 6731.85)$, [S II] spectral line width w, and $N(S^+)/N_e$ plotted against electron density and temperature under the assumption of thermal equilibrium. Owing to uncertainties in the geometry of the [S II] emitting volume, the curves of constant $N(S^+)/N_e$ must be interpreted as strict lower bounds on the S^+ density, with the most likely values of $N(S^+)/Ne$ about an order of magnitude larger than those lower bounds (see text). The shaded region corresponds to typical spectra, as discussed in § IVa.

IV. INTERPRETATION

a) The Thermal Plasma

We collect here the measured parameters pertinent to the temperatures and densities in the [S II] source region, and consider the case for a thermal plasma. The measured emission rates in both the λ6716 and λ6731 lines, together with an estimate of the plasma volume within our FOV, yields both the electron and ion densities and an electron temperature under the assumptions of thermal equilibrium and spatial homogeneity. Measured [S II] line widths yield independently an ion temperature for comparison with that of the electrons as a test for consistency. We assume that the plasma contains uniform densities and temperatures within our FOV, and therefore implicitly ignore the probable existence of spatial structure within the [S II] emitting regions, and derive representative values for the physical variables from integrals over the emitting volume.

Following well-understood procedures for the study of emission nebulae, we express the emission rate E in terms of the electron density N_e and temperature T_e in the form

$$E = N(S^+)LK(N_e, T_e) ,$$

where $N(S^+)L$ is the column density. We have recalculated the emissivities K for the observed [S II] lines using the values for the collision strengths given recently by Pradhan (1976) and the radiative probabilities of Garstang (1968). The results are given in Figure 5, which illustrates the relations between electron density and temperature, the measured doublet ratios DR = $E(6716)/E(6731)$, and the [S II] line width which constrains the electron temperature under the assumption of thermal equilibrium. The lines of constant T_e in the figure are related to the [S II] line widths w by the expression $T = mw^2/8k \ln 2$, where m is the mass of a S^+ ion. Also shown are constraints placed upon the ratio of densites $N(S^+)/N_e$ for an assumed $E(6731) = 50$ Rayleighs and L equal to the orbital radius of Io (5.9 R_J). Since $N(S^+)$ is proportional to $E(6731)/L$, interpolation from the illustrated curves provides the constraints for $E(6731)$ and L values other than those assumed.

Through Figure 5 we find the range of admissible densities N_e and $N(S^+)$ implied by our measurements. We consider the sequence of tracings 11.243–11.320, since in this sequence the doublet lines were measured alternately (three λ6716 scans intercalated between four λ6731 scans) and their strengths appear to vary smoothly over time (cf. Table 1 and Fig. 1). Averages and mean deviations for this sequence are $\bar{E}(6731) = 54 \pm 10$ Rayleighs, $\langle DR \rangle = 0.97 \pm 0.22$, and $\bar{w} = 5.1 \pm 1.3$ km s^{-1}. These values correspond approximately to the shaded region in Figure 5. In comparison, the averages for all the 33 λ6731 and 13 λ6716 scans are $\bar{E}(6731) = 44 \pm 4$ Rayleighs, $\langle DR \rangle = 0.98 \pm 0.07$, and $\bar{w} = 6.2 \pm 1.5$ km s^{-1}, which within their mean errors agree with those derived from the smaller sample.

With the values of $\langle DR \rangle$ and $\bar{w}$ listed above we may read off an electron density $N_e \sim 2000\ cm^{-3}$ from Figure 5 directly. The S^+ ion density may be estimated from the curves of constant $N(S^+)/N_e$ in the figure only after making an estimate for the fraction of the FOV–sampled volume occupied by the S^+ plasma. These curves, which correspond to the parameters of a uniformly illuminated FOV, define a firm lower bound on the S^+ density for [S II] source regions localized within the volume sampled by the FOV. Indications that the [S II] source was confined radially within the FOV (on the basis of observed line widths, § III*c*), and confined in latitude within the FOV (§§ III*a* and IV*b* below) suggest that no more than one-tenth of the FOV sample volume was filled. This means that the absolute surface brightness in the source region was an order of magnitude greater than the $E(6731)$ chosen for the computation of the figure, and $N(S^+)/N_e$ is estimated to fall between 10 and 90% by scaling from the curves in the figure.

Our assumption that the observed plasma is thermalized may be further checked for consistency. For an ion density $N(S^+) = N_e = 2000\ cm^{-3}$ and $T = 20{,}000$ K, the time for energy equipartition between electrons and ions is (Spitzer 1967, eqs. [5]–[31]) $t_{eq} = 6 \times 10^5$ s. In comparison, the recombination time of the S^+ ions is $t_{re} = [\alpha(T)N_e]^{-1} = 2 \times 10^8$ s, if the recombination coefficient $\alpha(T) = 3 \times 10^{-12}\ cm^3\ s^{-1}$ is adopted from Jacobs *et al.* (1979). If recombination were the only process determining the lifetime of an S^+ ion, then our assumption would be amply satisfied since $t_{re} \gg t_{eq}$. It is not clear, however, that this determines the S^+ lifetimes, since collisional ionization by thermal electrons and collective interactions related to the phenomenon of critical velocity ionization (Raadu 1978) may play a role. However, the same phenomenon of critical ionization will lead to equipartition in a time shorter than that evaluated from two-body interactions. The entirely different orders of magnitude between t_{eq} and t_{re} lead us to expect, nevertheless, that the plasma is thermalized.

We have found that the assumption of thermal equilibrium in the S^+ plasma leads to a self-consistent set of plasma parameters. Finally, we note that theoretical computations of the ionization balance in a thermal sulfur plasma predicts that S^+ is the dominant species for temperatures in the range 10,000–50,000 K (Jacobs *et al.* 1979). Further measurements bearing upon the ionization balance in the Jovian sulfur nebula will help clarify the details of the Jovian magnetospheric plasma evolution over time scales on the order of sulfur recombination times.

b) Equatorial Confinement

The spatial structure of the [S II] has been discussed in terms of a centrifugal confinement equator and angular separations in latitude φ_c from that equator. Here we define this geometry and discuss its applicability to ion confinement in the inner Jovian magnetosphere.

At the time of the *Pioneer* spacecraft encounters with Jupiter, the magnetic field within the radius of Io's orbit behaved nearly as expected for a dipole internal to Jupiter (Smith, Davis, and Jones 1975), and therefore the corotating thermal plasma did not induce significant distortions in the regions of the magnetosphere probed in our observations (Hill and Michel 1976). This is consistent with expectations based on the ratio between corotational kinetic energies and magnetic energy densities, since small values of this ratio (i.e., 1/50 at 5 R_J) ensure ion confinement along undistorted dipole force lines.

The observed thermal energies are, in turn, much less than corotational energies at the distance from Jupiter beyond a few R_J. Hill and Michel (1976) have derived an expression for the "scale height" of particles constrained by centrifugal forces as they spiral along the corotating magnetic dipole force lines. They show that the particle density $n(z)$ a distance z above the equator is $n(z) = n(0) \exp(-z^2/H^2)$, where the scale height H is given by

$$H = (2kT/3m\omega^2)^{1/2},$$

where kT is the thermal energy, m is the mass of the ion, and ω is the angular frequency for corotation. This reduces numerically to $H = 1.04 \times 10^{-3} T^{1/2}[R_J]$ for the S^+ scale height in units of R_J with T in degrees K. Thus S^+ ions at 20,000 K are confined within approximately $\pm 0.15\ R_J$ from the equilibrium latitude. A spin-aligned dipole geometry was assumed by Hill and Michel, but the derived scale height is not significantly altered by the tilt of the Jovian dipole.

The equilibrium latitude for ions moving along the corotating tilted dipole lines is given by the equation

$$\tan\theta = \frac{3}{2\tan\tau}\left[(1 + \tfrac{8}{9}\tan^2\tau)^{1/2} - 1\right],$$

where τ is the angle between radial lines in the rotational and magnetic dipole equatorial planes at a given longitude, and θ is the resulting angular separation between the rotational equator and the centrifugal equilibrium position (cf., Hill, Dessler, and Michel 1974). This equation simply specifies the position along a given dipole line of force which is most distant from the rotational axis. This expression reduces accurately to $\theta = (2/3)\tau$ for angles on the order of the Jovian dipole tilt, and therefore a centrifugal confinement equator is defined within a plane tilted two-thirds of the dipole tilt from the rotational equator. Using the 11° tilt of Smith, Davis, and Jones (1975) for the Jovian dipole, we find $\theta = 7°$; φ_c then measures the latitude separation from this tilted centrifugal equator.

As discussed in an earlier section, the distribution in [S II] emission rates against $|\varphi_c|$ at $\delta = 0.75$, as shown in Figure 3, indicates that the ions are confined within about 3° in latitude centered on the centrifugal confinement equator. At a radial distance of 5 R_J from Jupiter this implies confinement within $\pm 0.13\ R_J$. This is consistent with our expectations for a 20,000 K S^+ plasma as computed here, and

lends additional credence to our assumption of thermal equilibrium in the observed [S II] source region.

V. DISCUSSION

Our observations permit a coherent description of the Jovian magnetosphere at $\sim 5\ R_J$ probed by our [S II] observations during 1976 October 7–11. Our plasma parameters refer to a single point in time in the evolution of the Jovian magnetosphere, and establish an early point in our knowledge of the history of the Jovian thermal plasma.

Typical plasma parameters from our data include an equilibrium temperature of $\sim 20{,}000$ K, electron densities $\sim 2000\ \mathrm{cm}^{-3}$, and $N(S^+)/N_e \sim 10$–90% in a toroidal volume with cross-sectional dimensions of $\sim 0.3\ R_J$ at a distance near $5\ R_J$ from Jupiter. The toroid is inclined $\sim 7°$ to the rotational equator as expected for centrifugal confinement, and large-scale longitudinal structure in the [S II] brightness exists and persists over time scales of at least 10 Jovian rotations.

Although the measurements reported here were made long before the *Voyager 1* encounter with Jupiter (1979 March 5), there are several interesting points for comparison. The *Voyager 1* plasma experiment of Bridge *et al.* (1979) measured S^+ ion densities at two points (5.3 and 5.0 R_J) within the orbit of Io. S^+ densities of 1150 and 134 cm^{-3} are reported at these two points, respectively, and this may be interpreted as an indication of longitudinal variability in the S^+ densities, as would be expected on the basis of our [S II] observations. Although the S^+ densities in the local spacecraft vicinity clearly are capable of large variabilities, the densities appear to be consistent with the average densities we have observed. The *Voyager 1* Planetary Radio Astronomy experiment of Warwick *et al.* (1979) give evidence for electron densities up to about $2500\ \mathrm{cm}^{-3}$ in the vicinity of 5–6 R_J from Jupiter, which is clearly similar to the electron densities reported here. Our evidence for longitudinal structure warns against interpreting spacecraft measurements in terms of radial distance from Jupiter alone, as in the above report, but it is clear that the *Voyager* spacecraft and our ground-based observations describe similar magnetospheric phenomena. More recent Fabry-Perot observations of both [S II] and [S III] optical emissions were obtained near the time of the *Voyager 1* spacecraft encounter with Jupiter and are reported separately.

The presence of a S^+ plasma confined in an equatorial region strongly suggests that the sulfur source is likewise near the equator (Hill and Michel 1976), and on the basis of elemental composition Io is the obvious candidate. However, the details of the ionization, thermalization, and diffusion processes which maintain the observed S^+ plasma in a region distinct from Io's orbit are not understood. The data presented here, together with new ground-based and spacecraft-based observations now in various stages of completion, will fill many gaps in our knowledge of the Jovian plasma, and help establish a firm foundation for a description of the Jovian magnetospheric dynamics.

This work has been supported by NASA through grant NGL 05-002-003 to the California Institute of Technology and by NSF through grant GA 15733 to the University of Wisconsin.

REFERENCES

Acũna, M. H., and Ness, N. F. 1976, *Jupiter*, ed. T. Gehrels (Tucson: University of Arizona Press), p. 830.
Bridge, H. S., *et al.* 1979, *Science*, **204**, 987.
Brown, R. A. 1976, *Ap. J. (Letters)*, **206**, L179.
Bowen, I. S. 1955, *Ap. J.*, **121**, 306.
Garstang, R. H. 1968, in *IAU Symposium No. 34, Planetary Nebulae*, ed. D. E. Osterbrock and C. R. O'Dell (Dordrecht: Reidel), p. 143.
Hill, T. W., Dessler, A. J., and Michel, F. C. 1974, *Geophys. Res. Letters*, **1**, 3.
Hill, T. W., and Michel, F. C. 1976, *J. Geophys. Res.*, **81**, 4561.
Jacobs, V. L., Davis, J., Rogerson, J. E., and Blaha, M. 1979, *Ap. J.*, **230**, 627.
Kupo, I., Meckler, Y., and Eviatar, A. 1976, *Ap. J. (Letters)*, **205**, L51.
Münch, G., Trauger, J. T., and Roesler, F. L. 1977, *Bull. AAS*, **9**, 465.
Pradhan, A. K. 1978, *M.N.R.A.S.*, **183**, 89P.
Raadu, M. A. 1978, *Ap. Space Sci.*, **55**, 125.
Smith, E. J., Davis, L., and Jones, D. E. 1976, *Jupiter*, ed. T. Gehrels (Tucson: University of Arizona Press), p. 788.
Spitzer, L. 1967, *Physics of Fully Ionized Gases* (New York: Interscience), p. 135.
Trauger, J. T., and Roesler, F. L. 1972, *Appl. Optics*, **11**, 1964.
Warwick, J. W., *et al.* 1979, *Science*, **204**, 995.

GUIDO MÜNCH: Max-Planck-Institut für Astronomie, 6900 Heidelberg-Königstuhl, Federal Republic of Germany

F. L. ROESLER: Department of Physics, University of Wisconsin, 1150 University Avenue, Madison, WI 53706

JOHN TRAUGER: Division of Geological and Planetary Sciences, California Institute of Technology, 170-25, Pasadena, CA 91125